Dependence of 25-MHz HF Radar Working Range on Near-Surface Conductivity, Sea State, and Tides

MARK HALVERSON AND RICH PAWLOWICZ

Department of Earth, Ocean, and Atmospheric Sciences, University of British Columbia, Vancouver, British Columbia, Canada

CÉDRIC CHAVANNE

Institut des Sciences de la Mer de Rimouski, Université du Québec à Rimouski, Rimouski, Quebec, Canada

(Manuscript received 15 July 2016, in final form 28 October 2016)

ABSTRACT

A 1.6-yr time series of radial current velocity from a 25-MHz high-frequency radar system located near a coastal river plume is analyzed to determine how the working range varies in response to changing near-surface conductivity, sea state, and tides. *Working range* is defined as the distance to the farthest radial velocity solution along a fixed bearing. A comparison to spatially resolved near-surface conductivity measurements from an instrumented ferry shows that fluctuations in conductivity had the largest impact of the three factors considered. The working range increases nearly linearly with increasing conductivity, almost doubling from 19.4 km at 0.9 S m^{-1} to 37.4 km at 3.5 S m^{-1}, which yields a slope of 7.0 km per S m^{-1}. The next largest factor was sea state, which was investigated using measured winds. The working range increases linearly at a rate of 1 km per m s^{-1} of wind speed over the range of 0.5–6.5 m s^{-1}, but it decreases weakly for wind speeds higher than 7.5 m s^{-1}. Finally, a power spectrum of the working range time series reveals variability at tidal frequencies. Tides cause about 3 km of range variation; however, the mechanism(s) underlying this are not known explicitly. Evidence for both sea level height and the interaction of tidal currents with sea state are presented.

1. Introduction

The resonant scattering of high-frequency (HF) radio waves by ocean surface gravity waves was first explained by Crombie (1955), and this phenomenon was later exploited to build instruments to measure various ocean surface properties, such as currents (Stewart and Joy 1974; Barrick et al. 1977) and sea state (Hasselmann 1971; Barrick 1977). The HF radio spectral band refers to electromagnetic waves with frequencies ranging from 3 to 30 MHz; however, commercially available oceanographic HF radars make use of frequencies as high as 50 MHz. Electromagnetic waves at these frequencies couple to conductive surfaces, including land, freshwater, and seawater. These ''ground waves'' are trapped on the surface, which in principle allows for long-range measurements beyond the horizon because the waves follow Earth's curvature. However, in practice, natural waters are lossy media, and electromagnetic wave energy is lost by scattering and absorption. These factors—in combination with omnipresent HF band noise, both natural and electronic, and the loss from geometric spreading—place a practical limit on the range achievable by HF radar systems.

The dominant loss mechanisms at high frequencies in natural waters are absorption, which occurs as a result of its finite electrical conductivity, and the scattering of energy by a rough surface (i.e., by surface gravity waves). Both processes are fairly well understood theoretically, and a number of studies have partially verified the theory (section 2). However, there are very few studies that assess the impact of such losses on the distance over which reliable radial current measurements can be made, and those that do treat it in a cursory manner.

In this paper, we make use of data from a CODAR Ocean Sensors Ltd. SeaSonde 25-MHz radar system located in the Strait of Georgia, British Columbia,

Corresponding author e-mail: Mark Halverson, mhalvers@eos.ubc.ca

DOI: 10.1175/JTECH-D-16-0139.1

Canada. We analyze 1.6 years of radar data to determine how the distance to the farthest radial current solution, which Gurgel et al. (1999a) call working range, depends on conductivity, sea state, and tides. Our intent is to provide practical results under natural environmental conditions for an operational system, rather than undertaking a detailed study of path loss or signal-to-noise ratio (SNR) variability. The results here can be used as a guide to aid researchers in planning new systems, or understanding the limitations of existing systems. Readers interested in observational studies of path loss and SNR variability may consult the following references: sea state (Hansen 1977; Forget et al. 1982; Lyons and Barrick 1984), surface water conductivity (Forget and Broche 1991; Barrick and Long 2006), internal and external radio noise (Savidge et al. 2011; Meadows et al. 2013), and other instrumental parameters (Shearman 1983).

The Strait of Georgia is an ideal location to evaluate how the maximum range changes under various environmental conditions. First, the HF radar system overlooks the buoyant plume formed by the outflow of the Fraser River. Over the course of a year, the near-surface salinity (and therefore conductivity) of the plume varies dramatically. Second, it is relatively small and protected from the Pacific Ocean, so the surface wave field is locally generated. Thus, we can use local wind speed as a proxy for wave height. Finally, the Strait of Georgia has a relatively large maximum tide range of nearly 5 m, which, as we will show, has an impact on the working range.

2. HF radar ground-wave energy loss

a. Conductivity and frequency

The propagation of a high-frequency radio wave over the ocean surface depends strongly on the dielectric properties of the air and water. The complex relative permittivity ε at high frequencies is given by

$$\varepsilon = 80 + \frac{iC}{\varepsilon_o \omega}, \tag{1}$$

where C is the electrical conductivity, ω is the angular electromagnetic (EM) wave frequency, and ε_o is the absolute vacuum permittivity. Attenuation is governed by the imaginary component of ε, and because the effective impedance of the medium is inversely proportional to the relative permittivity, attenuation increases with EM wave frequency and decreases with conductivity (Barrick 1971a).

Seawater conductivity, in turn, depends on salinity, temperature, and pressure. The pressure dependence of conductivity is negligible in this study because the skin depth for EM waves at 25 MHz is on the order of a few centimeters (Barrick and Long 2006). Conductivity increases with increasing temperature and salinity in a way that is specified by the International Thermodynamic Equation of Seawater—2010 (TEOS-10) algorithms for the seawater equation of state (IOC et al. 2010).

The conductivity of seawater can change dramatically where changes in salinity are large, such as near the mouth of a river. Changes in salinity will attenuate the ground wave and therefore the SNR of the Bragg echo. This principle has been exploited by HF radar systems to track freshwater plumes (Forget and Broche 1991; Gurgel et al. 1999b).

b. Sea state

Retrieval of ocean currents by HF radar is based on the ability to detect Doppler shifts in scattered radio waves. Resonant, or Bragg, scattering occurs when the radio waves of wavelength λ are scattered by ocean waves with wavelength $\lambda/2$. Bragg scattering produces strong spectral peaks in the sea echo, with a frequency offset that depends on the surface wave phase velocity and the ocean current speed. These spectral peaks are referred to as the first-order Bragg peaks, and the ocean waves from which they scatter are called Bragg waves.

Sea state is another important marine environmental factor that determines the EM energy lost and thus the working range. A theoretical study by Barrick (1971b) predicted that EM wave energy loss increases with increasing wave height relative to a smooth surface for frequencies ranging from 2 to 50 MHz, with peak losses at about 10 MHz. Field studies generally confirm that energy is lost in proportion to wave height (Hansen 1977; Forget et al. 1982; Lyons and Barrick 1984).

However, in addition to scattering losses, surface waves influence the power received by changing the scattering cross section. First-order scattering theory (which produces the Bragg peaks) predicts that the scattering cross section of an EM ground wave from ocean surface waves increases with increasing sea state, implying that the working range should also increase (Gurgel et al. 1999a). Ultimately, the achievable range and its modulation by sea state will depend on the details of how both the scattering cross section and the scattering losses vary.

3. Study site, materials, and methods

a. Strait of Georgia and the Fraser River plume

The Strait of Georgia (SoG) is a midlatitude semienclosed coastal basin situated between mainland British Columbia and Vancouver Island (Fig. 1). It is a fjordlike system with two significant but physically

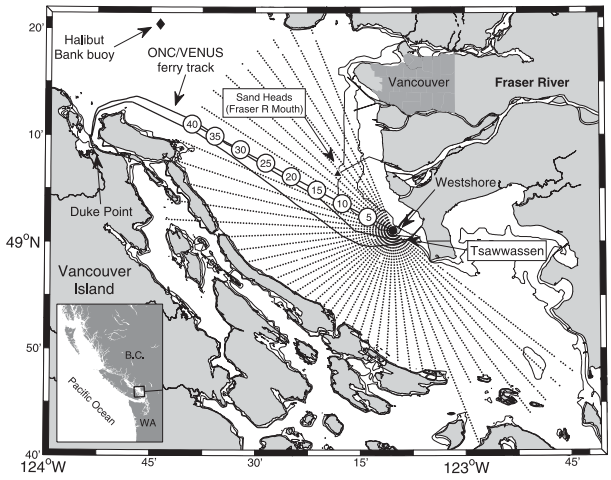

FIG. 1. Map of the lower Strait of Georgia illustrating the radial grid for the 25-MHz Westshore CODAR Seasonde (VCOL). The circled numbers represent distance along the bearing chosen for this study. The 5- and 20-m bathymetric contours are given by the thin lines. The ONC/VENUS (Victoria Experimental Network Under the Sea) instrumented ferry route, linking Tsawwassen in the southeastern SoG to Nanaimo on Vancouver Island, is shown by the solid line.

restricted entrances to the Pacific Ocean. The SoG is about 200 km in length, and between 20 and 40 km wide, and has an average depth of 140 m.

Freshwater from the Fraser River discharges into the southern Strait of Georgia near the city of Vancouver, Canada (Fig. 1), forming a buoyant and often turbid brackish plume. Freshwater from the Fraser River primarily mixes with seawater in the estuary and near-field plume (Halverson and Pawlowicz 2011), which ultimately forms a thin layer some 5–10 m thick. This brackish plume can extend for up to 20 km or more from the river mouth. The Fraser plume at any time of the year consists of the accumulation of about 2 days of tidally pulsed river outflow, mixed with saline SoG water (Halverson and Pawlowicz 2011). The mean salinity in the plume is well correlated with river flow at subtidal frequencies, such that high river flow results in a relatively fresh plume (Royer and Emery 1982; Halverson and Pawlowicz 2008). Superimposed on the low-frequency salinity response to river flow are relatively large fluctuations driven by the tides, which are modulated by the ≈14-day spring/neap and lunar declination tidal cycles (Halverson and Pawlowicz 2008). Northwesterly winds can advect the plume down the strait to the southeast, while southeasterly winds advect the plume up the strait to the northwest (Royer and Emery 1982).

Fraser flow is uncontrolled by dams, and its annual discharge cycle, as traditionally measured at the Hope, British Columbia (BC), streamflow gauge about 150 km upstream, is characterized by high flows during a summer freshet resulting from summer melting of the BC interior snowpack and much lower flows in winter. However, fall/winter rainfall events over the smaller coastal drainage basins downstream of Hope can add a substantial amount of freshwater for short periods.

Tides in the SoG are of the mixed type and characteristic of the temperate eastern Pacific. Tidal heights used in this paper were measured at Point Atkinson, BC, located 25 km north of the Fraser River mouth. Tidal records are available closer to the river mouth, but we sought a time series uncontaminated by the river stage. The total range in tidal heights over the study period is 4.7 m. Within the radar footprint for the data in this study, tidal currents are strongest near the Fraser River mudflats, reaching 25 cm s^{-1} for M_2, but they are generally 15 cm s^{-1} or less elsewhere (Halverson and Pawlowicz 2016). There is considerable spatial variability in the phase difference between the sea surface elevation and currents, suggesting baroclinic effects near the surface are important.

b. *HF radar*

Ocean Networks Canada (ONC) maintains an array of 25-MHz CODAR Ocean Sensors Ltd. SeaSonde units in the southern Strait of Georgia (Fig. 1). In this study we make use of data only from the Westshore Coal Terminal station (VCOL) because it has a number of radial azimuths that align with instrumented car ferry transects and pass directly over the brackish plume formed by the Fraser River. We initially examined data from the three azimuths closest to the ferry transects. There was essentially no difference in the working range between the three angles; thus, we selected the one nearest to the ferry track, which has a bearing of 298°T (Fig. 1).

All processing steps are accomplished with the CODAR processing software suite. The system configuration for this study is summarized in a radial file header included in the appendix. A few important parameters are noted here. A measured beam pattern was used in the processing. The SNR threshold for the first-order Bragg lines required to estimate a radial velocity from the spectra was set to 6.0 dB (RadialBraggNoiseThreshold = 4). The transmit bandwidth was 300 kHz (2 or 3 times larger than many systems), and the radial resolution was 0.5 km. The SpectraRangeCells parameter was set to 79 for the full period, which set the maximum possible range to 39.5 km. The radial velocity solutions were averaged in 5° azimuthal bins. Radial velocities are thresholded at 150 cm s^{-1}. Hourly radial current maps are formed by calculating the median velocity from seven 10-min averages. Targets placed over land are flagged and removed for this study.

A 1.6-yr period spanning 5 Jun 2014–23 Jan 2016 was chosen for the analysis. This period was sufficient to

characterize the dominant seasonal cycles of warming and freshwater input into the Strait of Georgia.

Working range is defined in this study as the distance from the antenna to the farthest radial velocity solution. Although this is a practical and conceptually straightforward definition, determining the range in practice is somewhat challenging for a few reasons. First, the multiple signal classification (MUSIC) direction-finding algorithm can leave small gaps in intermediate radial bins. Second, simply choosing the farthest bin is not a robust method for this system because the uppermost range limits often contained unphysical radial velocities, and the distance to spurious data is not a helpful definition of range. The unphysical radial velocities in these bins were associated with times when the first- and second-order lines blended together. The first-order line fitting algorithm did not reject these cases, and thus the radial velocity data in these bins are unreliable. Finally, if MUSIC places an incorrect velocity in the bin beyond the farthest radial (which should otherwise be empty), then the range will have been overestimated by 0.5 km.

A simple algorithm was designed to overcome some of the aforementioned difficulties. We determine the working range by advancing through the range bins until a significant spatial gap in radial velocity is reached, defined here as three or more bins. Smaller gaps were ignored because they failed to robustly determine the location of the farthest radial solution. On rare occasions, gaps of three bins occurred well within the range of good data, meaning that the range was underestimated in these cases. Increasing the gap threshold to three bins reduces these occurrences, but it has the unwanted side effect of causing the algorithm to more frequently reach the last possible bin. The impact of increasing the allowable gap to three bins on the bulk statistics of the working range is to increase the global average of the working range by just 0.1 km and to increase the standard deviation by a similar amount—negligible compared to the natural variability.

As will be shown in section 4e, the bins located beyond 37 km contain radial solutions more frequently than the adjacent bins at shorter distances; however, as discussed earlier, the velocities in these bins are often spurious. If the three adjacent bins (35.5–36.5 km) were empty, then the algorithm described above would have correctly ignored the spurious values. If the three adjacent bins contained radial velocities, then the algorithm returned a working range equal to the maximum possible range. These instances are not useful estimates of a working range, and the impact is that the system appeared to reach its maximum possible range more frequently than the statistics show. In the analyses to follow, we disregarded times when the system reached the maximum possible range (whether spurious or not) because these instances would bias the results.

c. Ferry sampling

In May 2012, Ocean Networks Canada installed oceanographic sensors on the M/V *Queen of Alberni*, a British Columbia Ferry Services Inc. vessel that services the Duke Point-to-Tsawwassen route in the Strait of Georgia (Fig. 1). This vessel crosses the Fraser River plume up to eight times per day. The track essentially runs along the strait, oriented to the northwest/southeast. A complete transect covers 70 km and takes 2 h. The section of the transect that lies beyond the maximum range of the HF radar system is discarded.

The oceanographic instruments are located in the engine room, and the source water is drawn from a dedicated port in the ship's hull, located midship, from a nominal depth of 2 m (Wang 2015). There is some uncertainty in this value because the depth can change depending on the ship's payload. Furthermore, Hinatsu et al. (2004) have shown that the effective sampling depth for such systems can be shallower than the water intake depth because surface waters are deflected downward as the vessel travels. A previous ferry sampling program in the Strait of Georgia, which was based on a vessel of a different design than that used in the current study, was shown to sample water from about 1.5-m depth despite the intake being at 3.5-m depth (Halverson 2009; Halverson and Pawlowicz 2011).

Data collection is automated by the YSI SeaKeeper Underway Sampling System, a self-contained collection of chemistry-free instruments. The system measures a variety of water properties (as well as meteorological data); however, we will use only conductivity and temperature records, which are measured by a Sea-Bird Electronics SBE45 MicroTSG thermosalinograph at 10-s intervals. Salinity will be given in terms of the TEOS-10 Reference Salinity (S_R), which can be thought of as the Absolute Salinity (S_A) with $\delta S_A = 0$ (although it can be as large as $0.1\,\mathrm{g\,kg^{-1}}$ near river outflows; Pawlowicz 2015). Reference Salinity was chosen because it is based on conductivity and therefore meaningful to EM wave propagation, and also because the composition anomaly δS_A is not known for the Strait of Georgia.

d. Fraser River discharge

Most references to the Fraser River flow refer to the discharge measured at the Water Survey of Canada's Hope gauge station (ID 08MF005). It lies 120 km upstream of the mouth and is the nearest active station to the mouth that does not experience tidal fluctuations. Pawlowicz et al. (2007) have shown that the discharge at the Port Mann bridge (ID 08MH126), 35 km upstream of the mouth and downstream of all major tributaries, can exceed the Hope discharge by 20% in the summer

and nearly 100% in the winter. However, discharge at Port Mann is not available for the time period in this study, and the regression in Pawlowicz et al. (2007) that attempts to model this is appropriate for discharge on weekly scales, whereas we require data that capture daily variability.

Another simple method to account for Fraser River tributaries downstream of Hope was developed in Halverson and Pawlowicz (2008). Here we follow that method but make some adjustments because the largest tributary downstream of Hope is no longer gauged. Instead, we will scale up the Chilliwack River discharge (ID 08MH001) to account for all of the input downstream of Hope. The Chilliwack River is useful for this purpose because it contains hydrometeorological signatures of both the early summer snowmelt freshet and the rainfall events common throughout fall, winter, and spring (Halverson and Fleming 2015).

e. *Meteorological data*

The nearest source of meteorological data to the Fraser River plume is the Sand Heads lighthouse station, Environment and Climate Change Canada (ECCC) Climate ID 1107010, which is positioned at the end of the jetty at the mouth of the Fraser River (Fig. 1). The hourly wind speed is a 2-min average measured at an elevation of 11 m. The height is adjusted to 10 m using the parameterization of Smith (1988).

The ECCC Halibut Bank wave and weather buoy (C46146) provides spectral wave energy distribution, wave period, and significant wave height, as well as standard atmospheric parameters at hourly intervals. The buoy is moored 50 km northwest of the HF radar. The wind speed is measured at 5 m, but it is adjusted to a height of 10 m using the parameterization of Smith (1988).

4. Results

a. *Characterizing the working range time series*

A 1.6-yr time series of the working range, along with Fraser River discharge and near-surface conductivity, measured the wind speed at Sand Heads, and the tidal elevation at Point Atkinson is displayed in Fig. 2. The working range varies from about 8 to 39.5 km—the maximum possible upper limit as defined by the instrument configuration. The working range reaches its maximum in 14% of the observations, although the radial velocities at these distances are not necessarily reliable. After removing those instances of maximum range, the mean working range for the dataset is 28.6 km, while the standard deviation is 6.0 km. The working range probability distribution function is negatively skewed, meaning large values are more common than small values.

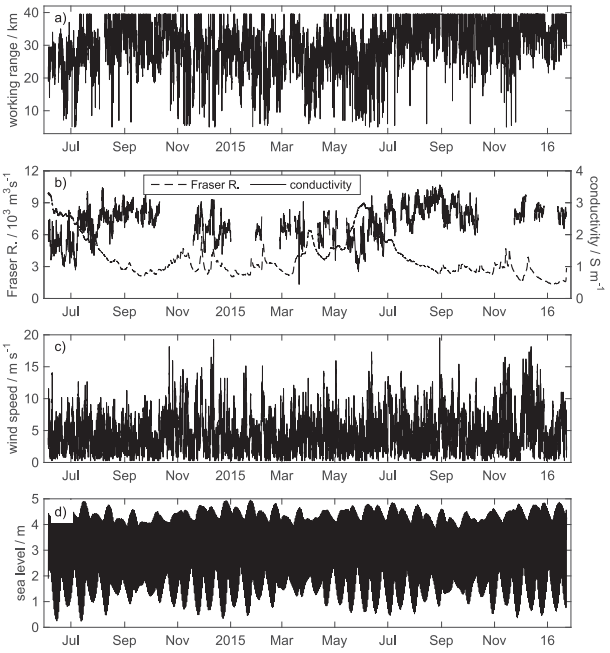

FIG. 2. Time series of (a) working range, (b) near-surface conductivity and Fraser River discharge estimated at the mouth, (c) wind speed at Sand Heads lighthouse station, and (d) measured sea level at Point Atkinson. Wind speed is a proxy for sea state, for which there are no measurements in the HF radar footprint.

The working range time series contains variability on time scales ranging from tidal to annual. The annual cycle of the working range is characterized by generally low values during the June–August period, which corresponds to times of high river flow (Fig. 2b). High river flow periods correspond to relatively fresh near-surface waters in the Fraser River plume (Royer and Emery 1982; Halverson and Pawlowicz 2008), which in turn means the conductivity is relatively low. In the next section we will quantify the degree to which the range is determined by surface water conductivity.

The relatively long data record displayed in Fig. 2 makes is difficult to identify the source of the high-frequency variability, which we presume for the moment is driven by wind and tides. To illustrate the correlation between wind speed and tides with range, consider Fig. 3, which displays 29 days of data from June/July 2015. This period demonstrates clear evidence of both tide- and wind-driven variability. For example, consider the strong wind event that occurred from 1 to 5 July 2015, which had wind speeds exceeding 10 m s^{-1}. During this time, the system consistently achieved high values of the working range—even reaching the maximum possible range of 39.5 km at times. This is also a period of spring tides, and the working range contains what appear to be tidal fluctuations. In the sections to follow, we examine the high-frequency variability in detail.

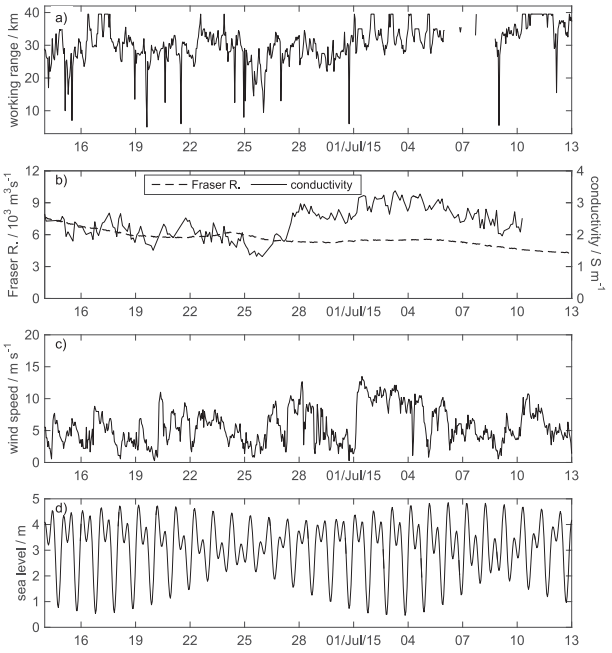

FIG. 3. Expanded view of Fig. 2 to illustrate the effect of wind and tides on working range.

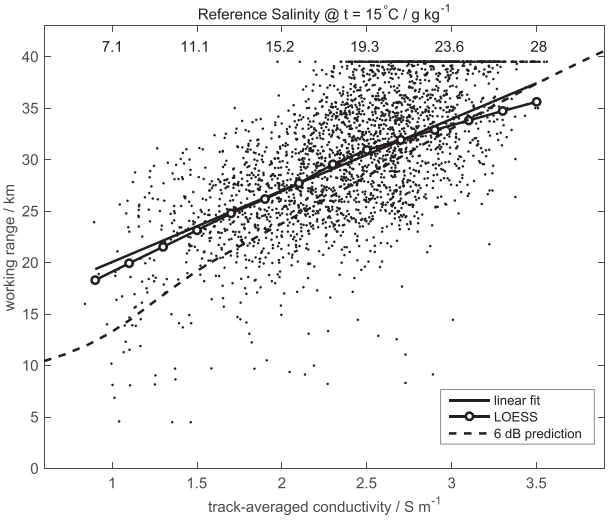

FIG. 4. Regression of track-averaged in situ conductivity with working range. The solid line with open circles was computed with the LOESS algorithm, a nonparametric curve smoothing technique. The thick solid line is a least squares fit to a simple slope and intercept. The instances where working range reached the maximum are included in the scatterplot but were removed when computing the fits. The dashed line is the theoretical prediction for 6-dB SNR at $t = 15$°C from the model of D. Barrick and R. Long (2006, unpublished manuscript).

b. *Seawater conductivity*

The working range tends to be relatively low when the Fraser River discharge is high and when the near-surface conductivity is low (Fig. 2). The causal relationship between range and river input is straightforward. First, the average near-surface salinity of the Fraser River plume is inversely related to river discharge at low frequencies (i.e., more than a few days; Halverson and Pawlowicz 2008). Second, seawater conductivity is proportional to salinity for a given temperature. Third, the attenuation of an EM wave at 25 MHz is inversely proportional to conductivity [Eq. (1)]. These relationships predict that the EM ground-wave energy lost will increase with river flow, thereby reducing the working range.

A direct regression of near-surface conductivity, formed by averaging ferry transects, versus working range indicates that the working range increases with increasing conductivity, as expected (Fig. 4). The relationship has considerable variability, but we will show in the next sections that at least some of this variability is caused by the tides and changes in sea state. Here we effectively smooth these variations by fitting a line to the data with the least squares method. The resulting line reaches from 19.4 km at $C = 0.9\,\mathrm{S\,m^{-1}}$ to 37.4 km at $C = 3.5\,\mathrm{S\,m^{-1}}$, which produces a slope of 7.0 km per $\mathrm{S\,m^{-1}}$. Fitting a nonparametric curve with a locally weighted scatterplot smoothing algorithm (LOESS) suggests that the conductivity–range relationship has some curvature, particularly at high conductivity, but it shows that the linear regression closely approximates the data trend. The linear correlation coefficient between conductivity and range is 0.58, which means that the conductivity explains 34% of the variance in working range.

To provide a more practical result, we also regressed the working range with in situ salinity (not shown; however, Fig. 4 includes a second x axis for Reference Salinity at $t = 15$°C). In doing so, it is important to note that conductivity is also a function of temperature, and the observed near-surface temperature in the Fraser River plume varies seasonally from about 5° to 20°C (Halverson 2009). At $S_P = 25$, the difference in conductivity over this temperature range is $1\,\mathrm{S\,m^{-1}}$, which introduces additional variability to the regression. A least squares fit of the working range to Reference Salinity yields a line that increases from 19.5 km at $S_R = 5.0\,\mathrm{g\,kg^{-1}}$ to 37.6 km at $S_R = 30.0\,\mathrm{g\,kg^{-1}}$, which yields a slope of 0.7 km per $\mathrm{g\,kg^{-1}}$.

c. *Sea state*

Evidence for the importance of wind (and thus waves) can be found in Fig. 3, which shows that the range can be relatively high, even reaching the maximum value, during windy periods. This is true even for times when the Fraser River flow is relatively high, and thus the

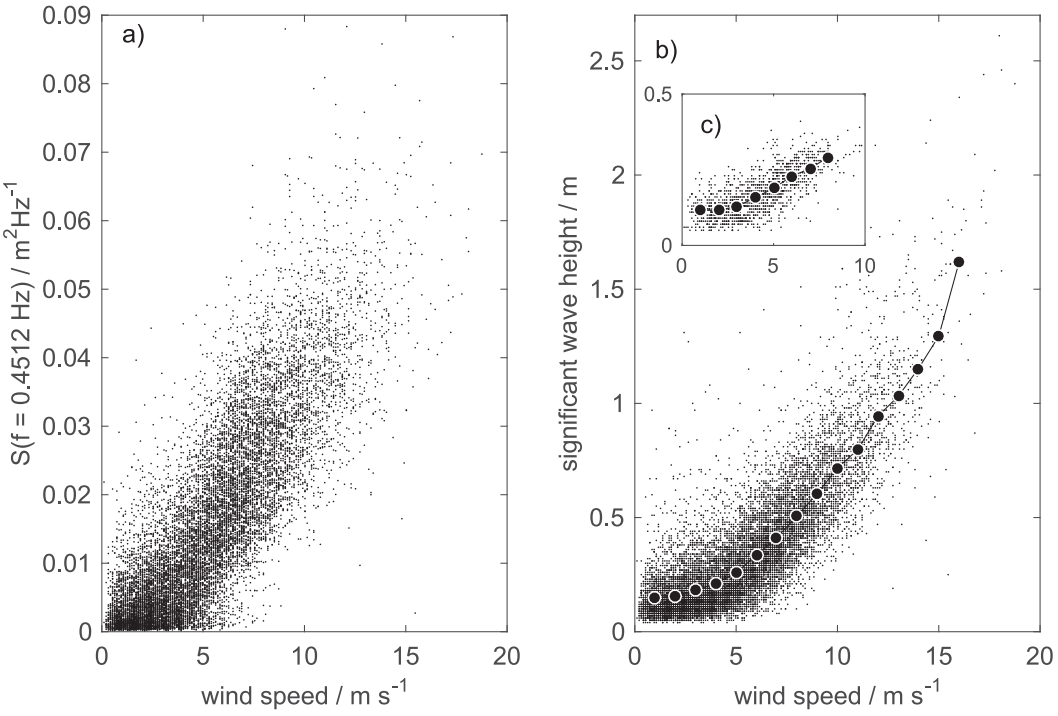

FIG. 5. Regression of (a) wind speed with wave spectral energy density $S(f)$ at $f = 0.4512$ Hz, and (b) wind speed with significant wave height, and (c) wind speed with significant wave height for times when the dominant period was 2.22 s (to match the Bragg wavelength). The larger black dots in (b) and (c) represent the averages in 1 m s^{-1} bins. Data were measured by the ECCC Halibut Bank wave buoy, located 50 km northwest of the Westshore HF radar site (Fig. 1).

surface conductivity is low, which is apparent during a wind event from 5 to 8 Feb 2015. Examples of the system achieving high values of working range can also be found during windy periods occurring in the early summer freshet, when the surface waters are very fresh.

To quantify the impact of sea state, the working range should be compared to coincident measurements of sea state. Unfortunately there are no direct wave measurements within the Westshore radar domain. However, an analysis of the wind and wave records from the ECCC Halibut Bank weather buoy, 50 km northwest of the Westshore radar site, shows that wind is a good proxy for sea state under the fetch and wind conditions observed in the SoG. Unfortunately, we cannot use the record as a direct characterization of sea state in the radar footprint because the orography near the Halibut Bank buoy differs from the radar domain.

The spectral energy at the Bragg wavelength provides a measure of the surface wave scattering cross section (for the moment we are ignoring directional effects). The highest frequency sampled by the wave buoy is $f = 0.4512 \pm 0.1016$ Hz, which is slightly lower than the frequency of the 6-m Bragg waves (0.5 Hz) observed by the HF radar system. Observed wave spectral energy at $f = 0.4512$ Hz increases approximately linearly with wind speed, although the relationship is also affected by other parameters, such as fetch or wind duration (Fig. 5a). Significant wave height H_s gives an indication of the scattering loss because it is proportional to the integral of the wave spectrum. It increases with wind speed in an approximately parabolic fashion (Fig. 5b). Although significant wave heights reach as high as 2.5 m, 97% of all hourly values are below 1 m—consistent with previous observations made nearer to the radar footprint (Meulé et al. 2007). The dominant periods associated with the significant wave heights are generally longer than the period of the Bragg waves. If the buoy record is filtered for times when the dominant period is 2.22 s (i.e., 1/0.4512 Hz) and we regress the associated significant wave height with wind, we see that these waves also increase with wind speed, but that they have a much smaller amplitude (<0.4 m; Fig. 5c).

To estimate the impact of surface waves on range, we calculate conditional averages of the working range in a number of wind speed bins using the wind speed measured at Sand Heads. A high-pass filter is applied to the range time series with a 20-day Blackman window to minimize low-frequency river discharge effects. Ideally, we would also remove the tidal signal, but the wind likely produces some high-frequency variance that

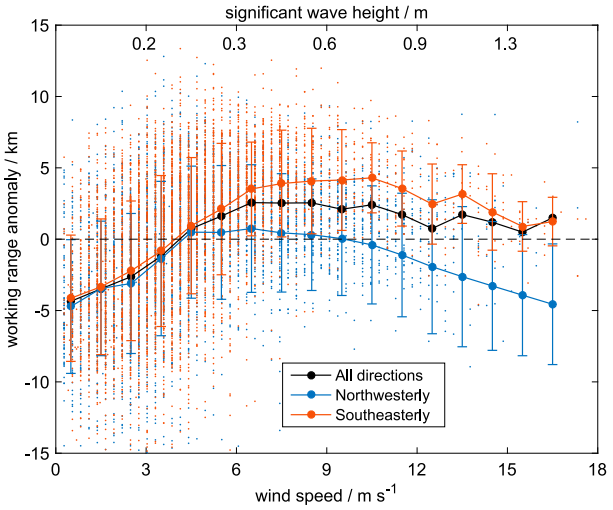

FIG. 6. Working range anomaly as a function of wind speed measured at Sand Heads, a proxy for surface wave amplitude. The range time series was low-pass filtered to remove low-frequency (≳20 days) conductivity fluctuations caused by the Fraser River. Error bars represent plus/minus one standard deviation of the data within each bin. Significant wave height is an estimate based on the empirical relationship between wind speed and wave height measured at Halibut Bank shown in Fig. 5b.

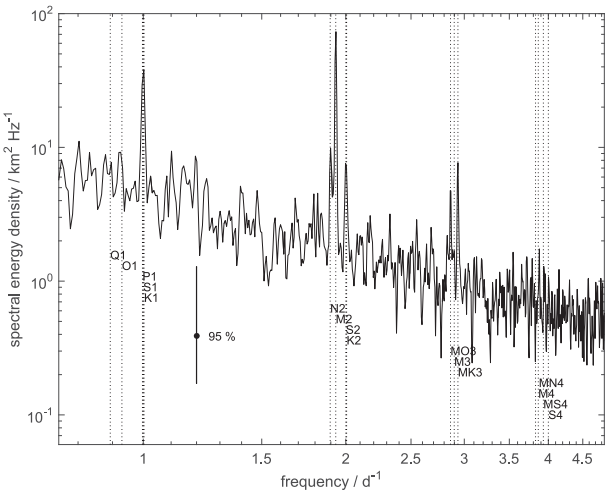

FIG. 7. Power spectrum of working range using Welch's overlapped segment method. Eight windows overlapped by 50% yields about 15 degrees of freedom and window lengths of 150 days. The vertical lines indicate astronomical tidal frequencies for major diurnal, semidiurnal, terdiurnal, and quarterdiurnal constituents.

would be removed by a tide-eliminating filter (e.g., sea breeze and S_1). Bin averaging by wind speed can effectively remove the tidal signal because the wind and tide records are not correlated. The result is that the range anomaly varies nonlinearly with wind speed (Fig. 6). At low wind speeds, from 0.5 to 6.5 m s^{-1} ($H_s < 0.5$ m), the range anomaly increases linearly from −4 to 2 km. At higher wind speeds, the range anomaly increases more slowly, eventually reaching a maximum of +2.5 km at a wind speed of 7.5 m s^{-1} ($H_s \approx 0.5$ m). At the highest wind speeds, the range anomaly declines weakly; however, the variability is high and there are fewer data points, so the decrease is only weakly statistically significant. The bin-averaged curve explains 16% of the variance of the working range time series.

The wave conditions experienced in this region depend somewhat on the wind direction because it determines the fetch (Meulé et al. 2007). The fetch is largest under northwesterly winds, so under these winds wave heights should be maximized for a given wind speed. Furthermore, the backscatter cross section of an EM wave from surface gravity waves depends on their directional distribution (Gurgel et al. 1999b). Both of these factors raise the possibility that the wind direction may have some bearing on the working range. Repeating the analysis above but selecting only for northwesterly winds ($270° \leq \theta \leq 360°$) reveals that the range anomaly is lower compared to the all-winds average by as much as 3 km. Under southeasterly winds ($90° \leq \theta \leq 180°$), the range is as much as 2 km higher than the all-winds average. The difference in the working range between the two wind direction cases therefore can reach 5 km, but significant range differences do not occur until the wind speed exceeds about 6 m s^{-1}.

d. *Effect of tides*

The time series of the working range in Fig. 3 contains variability on scales of days or less, raising the possibility that tides have an effect. To determine whether these high-frequency fluctuations are related to the tide, we compute the Welch periodogram of the range time series and search for variance at the known tidal frequencies. As suspected, the periodogram reveals enhanced energy at a number of discrete frequencies (Fig. 7). These frequencies correspond with some of the main tidal constituents important in the SoG, including M_2, N_2, S_2/K_2, $K_1/S_1/P_1$, and a few shallow water constituents. A slash (/) indicates that these constituents could not be isolated in the Welch periodogram. The 150-day window used is not sufficiently long to resolve S_2/K_2 and $K_1/S_1/P_1$; however, when the spectral energy density is estimated with a periodogram, providing the highest frequency resolution, the energy in these groups occurs mostly at the frequency of S_2 and S_1.

A harmonic tidal analysis shows that fluctuations at the astronomical tidal forcing frequencies account for 14% of the total variance but with the caveat that some of this energy is not tidal in nature. For example, the $K_1/S_1/P_1$ peak is centered on S_1. This constituent is very

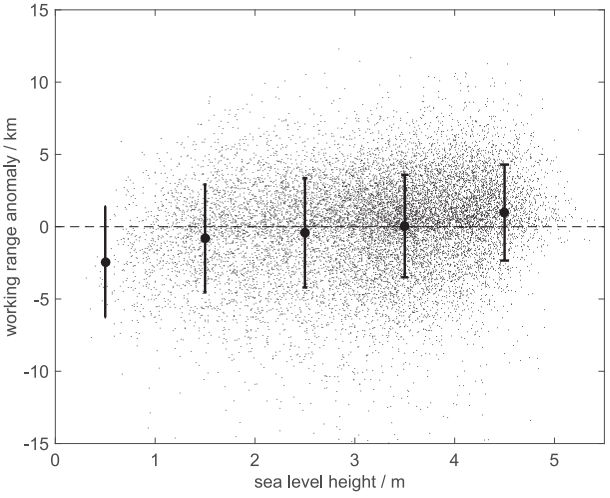

FIG. 8. Working range anomaly as a function of sea surface elevation (meters above chart datum). The vertical lines represent plus/minus one standard deviation about the mean of the data within $\Delta\eta = 1$ m bins.

weak in the SoG sea level record, and we argue later that it is caused by sea breeze. At any rate, the significant spectral energy at M_2 and N_2 confirms that at least some of the high-frequency variability in the working range time series is caused by the tides.

The sensitivity of the working range to the tides observed here is the first known report of this phenomenon. The mechanisms that might link tides to working range are not immediately obvious, unlike the link between range and conductivity. Here we take the first steps in determining the link(s) by first noting that there are two important aspects of the tides—sea level and currents.

We first check whether the tidal variation of the sea level is important by high-pass filtering the working range time series to remove the contribution of low-frequency river discharge forcing. We then form conditional averages of working range within a series of sea surface elevation bins using the measured sea level at Point Atkinson (Fig. 8). The result is that the range anomaly correlates weakly with elevation, increasing from −2 km at the lowest tides ($0\,\text{m} < \eta \leq 1\,\text{m}$) to +1 km at the highest tides ($4\,\text{m} < \eta \leq 5\,\text{m}$). The systematic increase of range with sea level exists within a considerable amount of scatter; however, the increase with elevation is statistically significant. For example, the average range anomaly in $2\,\text{m} < \eta \leq 3\,\text{m}$ is statistically lower than the average range anomaly in $3\,\text{m} < \eta \leq 4\,\text{m}$. While the differences are small compared to the scatter, the volume of data makes the standard errors in each bin small. The scatter is likely partly due to the incomplete removal of sea state effects. The technique used here was to high-pass filter the original time series with a 51-h Blackman window, which passes the tidal energy but likely also permits some high-frequency wind energy. Despite the noise it is at least plausible that some of the tidal variance is explained by the sea level itself.

Tides also drive an oscillatory flow in the Strait of Georgia, so we might ask whether tidal currents have an impact on working range. Some support for this idea stems from the observation that the linear correlation coefficient between sea surface height and working range is highest when the sea surface is lagged by about 1.5 h (i.e., range leads sea surface). A cross-spectral analysis reveals that the coherence is strongest in the semidiurnal band near M_2 and that the corresponding phase difference is consistent with the lagged correlation. The barotropic tide in the Strait of Georgia is primarily a standing wave (Thomson 1981), which implies that the tidal currents peak midway between low and high water. However, the surface tide Greenwich phase in the radar footprint departs somewhat from the barotropic tide (Halverson and Pawlowicz 2016), meaning that if there were a link between the tidal currents and range, then the phase difference would not necessarily be 3 h. The phase difference between range and sea surface elevation is not caused by the fact that Point Atkinson is 35 km north of the HF radar station because the sea level phase difference between these sites for M_2 is just a few degrees (Foreman et al. 1995).

e. *Statistical approach to working range*

An alternative approach to study the variability of working range is based on calculating the return rate, defined here as the percentage of time each radial bin contains a radial velocity solution. One reason for doing this is to check whether the same conclusions about the impact of conductivity and sea state on range are reached without needing to determine the maximum working range explicitly.

A plot of range versus return rate using the full dataset shows that, in general, the rate decreases with increasing range (Fig. 9). Low values are achieved in range cells near the transmitter because of the blanking period. The return rate is greatest at 93% at $R = 4$ km. At farther distances, it declines slowly to about 85% at $R = 20$ km. Beyond $R = 20$ km, the rate decreases quickly and eventually reaches a minimum of 14% at $R = 36.5$ km. Beyond this the return rate rises quickly; however, the radial velocities measured here are often spurious.

As with the working range time series, we can conditionally average the data to determine whether and how conductivity and sea state—represented by river flow and wind speed, respectively—impact the chances of

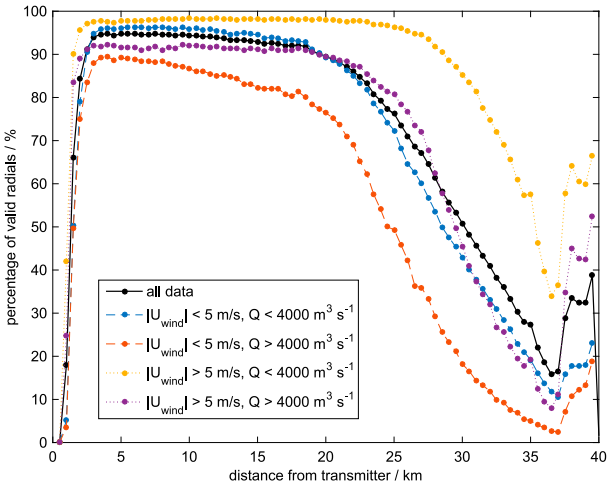

FIG. 9. Percentage of valid radial current solutions as a function of distance from the transmitter. The increase in return rate in the farthest range bins likely indicates that many radial velocity estimates exceeding 37 km are probably not reliable (section 3b).

obtaining a radial solution. We ignore tidal fluctuations for this analysis because the tide influence is weak. As might have been expected, the combination of high wind speed, defined as $U_{10} > 5\,\mathrm{m\,s^{-1}}$, and low river flow, defined as $Q < 4000\,\mathrm{m^3\,s^{-1}}$, produces the greatest chance of determining a solution in every range cell. In contrast, the combination of low wind speed and high river flow produce the lowest odds of finding a radial solution for all ranges. The discrepancy between these cases increases with distance. The other two cases—high wind plus high river flow and low wind plus low river flow—produce curves that are similar to the grand average. Thus, the increased propagation loss occurring during high-river-flow conditions (low conductivity) can be offset by windy periods (large waves). Furthermore, wind and river flow have a roughly similar influence on the working range, at least over the conditions found in the Strait of Georgia and defined by our averaging criteria.

5. Discussion

a. Summary of observations

In this paper we have identified three factors that affect the working range of a 25-MHz radar system for radial current measurements: seawater conductivity, sea state, and tides. Of these three factors, conductivity has the largest impact because of the large variations in near-surface salinity caused by the Fraser River. The dominance of conductivity is not expected to be a general result because most HF radar installations do not overlook the outflow of a large, highly seasonal river. The range increases linearly with conductivity from 19.4 to 37.4 km at a rate of 7.0 km per $\mathrm{S\,m^{-1}}$. The linear approximation explains 34% of the variance in the working range time series.

The second-most important factor affecting range is sea state, which is represented by hourly local wind speed in this study. Wind speed accounts for 16% of the total variance in working range. The working range increases by 7 km as wind speed increases from 0.5 to $6.5\,\mathrm{m\,s^{-1}}$; however, at higher speeds, the range levels off and eventually decreases slightly. Wind direction becomes important to working range at wind speeds above about $6\,\mathrm{m\,s^{-1}}$ because wind direction determines fetch. The shortest ranges for wind speeds above $6\,\mathrm{m\,s^{-1}}$ are achieved during northwesterly winds.

Direct wave measurements are not available within the radar footprint, but data from the Halibut Bank wave buoy suggests that the significant wave height that maximizes the working range at a given conductivity is in the range of 0.4–0.9 m. When the wave field has a peak period of 2.2 s (near the Bragg period), the significant wave height is usually in the range of 0.1–0.2 m (Fig. 5c). In terms of the wave field at the Bragg frequency, peak ranges are attained when wave spectral energy density is in the range of about $0.2–0.4\,\mathrm{m^2\,Hz^{-1}}$.

While conductivity is the dominant factor that limits working range, a relatively good range of 30 km can still be achieved during periods of low surface water conductivity ($C \approx 2\,\mathrm{S\,m^{-1}}$) under modest wave conditions ($H_s \approx 0.6$ m). This observation reflects the findings of Meadows et al. (2013), who find the range achieved by both 5- and 42-MHz systems to be highly dependent on wave conditions in Lake Michigan, for which the conductivity is two orders of magnitude lower.

The combined effects of conductivity and sea state can be summarized by an objective map (Fig. 10). This map shows that the response of range to wind speed is not linear, while the response to conductivity is nearly linear (at least over the range of conductivity observed). The range generally peaks at wind speeds of about $6–8\,\mathrm{m\,s^{-1}}$ ($H_s \approx 0.5$ m) but only for $C > 2\,\mathrm{S\,m^{-1}}$. At lower conductivity it is not clear whether this relationship holds because instances of high wind speed (more common in winter) with very high river flow (which occurs in summer) are rare. Even so, it is clear that the lowest range is achieved when the conductivity is low and when the wind is calm, and that the highest range is achieved when the conductivity is high and the wind speed is between about 6 and $8\,\mathrm{m\,s^{-1}}$.

Finally, a power spectrum of the range time series shows that the range time series contains fluctuations at known tidal frequencies, especially those known to be important in the Strait of Georgia. A harmonic analysis reveals that 14% of the total variance occurs at tidal

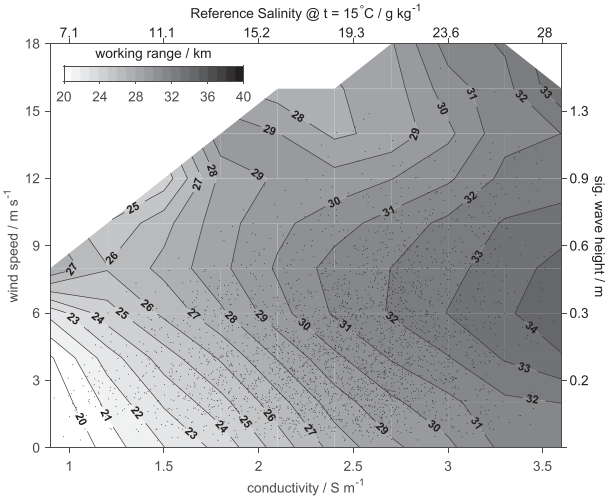

FIG. 10. Objective map summarizing the dependence of working range on both surface water conductivity and wind speed. The data points are included to indicate the data density.

frequencies; however, this is the upper limit of what can be attributed to tidal effects because the energy at S_1 is not tidal in nature. When we directly estimate the degree to which the tidal component of sea surface height affects the range, we see evidence of an increase of only 3 or 4 km as the sea level increases from 0 to 5 m. As noted earlier, the phase difference between range and sea level suggests that the range varies in phase with the tidal currents. We now consider each effect in more detail.

b. *Surface water conductivity*

The importance of finite conductivity to ground-wave energy loss is a basic result of the theory of EM wave propagation. This has been explicitly addressed in the ocean in a few instances. Forget and Broche (1991) validate the theoretical prediction results using measurements of path loss at 47.8 MHz in an estuary with variable conductivity. Barrick and Long (2006) observe a reduction in working range in two 42-MHz CODAR SeaSonde systems in San Francisco Bay following a rapid freshening of the surface waters. The reduction was attributed to the decrease of surface water conductivity.

Barrick and Long (2006) summarize the basic physics behind the impact of finite conductivity on ground-wave propagation and then model the reduction in working range as a function of threshold Bragg peak signal-to-noise ratio, radar frequency, and surface salinity. We use that model here to predict the working range as a function of conductivity, for the particular case of 25 MHz and a threshold Bragg SNR of 6 dB [note that Barrick and Long (2006) use salinity in place of conductivity by assuming $t = 15$°C]. The result is included on the scatterplot of working range and conductivity in Fig. 4. The predicted range increases nonlinearly from 17 km at $C = 1.3\,\mathrm{S\,m^{-1}}$ to 37.5 km at $C = 3.5\,\mathrm{S\,m^{-1}}$. It agrees very closely with the observations at higher conductivity; however, at the lowest conductivity the model underpredicts working range by about 5 km.

On the average, the model predicts a lower range, and one reason for this might be due to how the model represents sea state. It uses a Phillips-type wave energy spectrum having a significant wave height of 2 m. Such a wave spectrum is not generally appropriate for fetch-limited waters, and significant wave heights in the SoG rarely reach 2 m (Fig. 5). Scattering loss increases with wave height, which decreases the signal-to-noise ratio and therefore the working range.

We also note that the conductivity measurements made by the ferry-based sensors sample water at a nominal depth of 2 m (Wang 2015), which is deeper than the EM wave skin depth. Because of the large input of freshwater from the nearby Fraser River, the surface layer can be stratified to the surface, meaning that the surface salinity, and therefore conductivity felt by the EM waves, is likely lower than the ferry measurements. The difference will depend on the freshwater input, proximity to the river mouth, and winds, but extrapolating near-surface salinity profiles shown in Fig. 3 of Halverson and Pawlowicz (2011) to the surface could yield a decrease of S_R of 0–3 $\mathrm{g\,kg^{-1}}$ or more, and therefore a conductivity decrease of up to $0.35\,\mathrm{S\,m^{-1}}$ at $t = 15$°C. This would effectively lessen the slope of the range–conductivity relationship in Fig. 4 because the stratification is proportional to the salinity at 2 m.

c. *Sea state*

Wind speed explains only 16% of the total variance in the working range time series despite the robust increase at low wind speeds. The relatively low variance explained arises from the weak dependence of range on wind speed above $6.5\,\mathrm{m\,s^{-1}}$ and the relatively high level of noise in the scatterplot. While some of the noise is caused by tidal variations, much of it is likely caused by the choice of using wind speed to represent sea state. The variability in the relationship between wind speed and sea state in Fig. 5 implies that wind speed is an imperfect predictor of sea state, presumably because of complications such as the directional dependence of fetch and wind duration. Therefore, some of the variability in the relationship between wind speed and wave height will cause variability in the relationship between wind speed and working range.

Additional uncertainty in the relationship between wind and working range arises because the wind direction affects near-surface conductivity sampled by

the SoG Westshore HF radar system. Halverson and Pawlowicz (2016) have shown that the salinity along the ferry track, which coincides with the radar bearing analyzed in this study, depends on the wind direction, which is caused by advection of the Fraser River plume. If, for example, the plume is advected to the southeast by northwesterly winds, then the salinity and conductivity along the ferry track will increase, meaning that the range should increase. However, northwesterly winds have the effect of decreasing the range slightly, which contradicts the expectation of reduced loss from high-conductivity waters.

Practical assessments of the impact of sea state on working range have been made in a few HF radar systems. Gurgel et al. (1999a) observe the working range to decrease with increasing significant wave height for a 30-MHz beam forming system located in the North Sea. Cosoli et al. (2010) also observe a decrease in range with increasing significant wave height for a 25-MHz CODAR system in the Adriatic Sea. In contrast, Kamli et al. (2016) observe an increase in range as spectral energy (at the Bragg wavelength) increases in a 13-MHz CODAR system in the Lower St. Lawrence estuary. At higher wave energy, the range approaches a constant.

The increase of working range with wave height observed here stands in direct contrast to the observations of Gurgel et al. (1999a) and Cosoli et al. (2010), but it agrees qualitatively with the observations of Kamli et al. (2016). We suggest that the apparent contradiction might be resolved by noting that the observed wave heights reached 4 and 3 m in the Gurgel et al. (1999a) and Cosoli et al. (2010) studies, respectively, whereas significant wave heights rarely exceed 1 m in the SoG (Fig. 5). The Kamli et al. (2016) study also takes place within a fetch-limited region, and observed significant wave heights were 1 m or less.

The variable response of range with wind found in these studies likely reflects the interplay of the two competing roles that surface waves play in HF radar sensing of the sea surface. The first consideration relates to energy loss. Theoretical treatment of EM wave propagation over a rough conducting surface predicts that the ground-wave energy loss is proportional to sea state (Barrick 1971b). Field studies have confirmed this over a range of radar frequencies (Forget et al. 1982; Lyons and Barrick 1984). Based on this argument alone, the working range should decrease with wave height because more energy is lost, reducing the signal strength. The second consideration relates to scattering strength. HF radar current measurements rely on the strength of a scattered signal, and thus any dependence of scattering cross section on sea state must also be considered. Gurgel et al. (1999b) notes that the first-order backscatter cross section is proportional to the Bragg wave spectral energy density, which in the absence of other factors means that the working range should increase with sea state. Therefore, surface waves both help and hinder ocean current retrieval by HF radar. Waves must be present because HF radar relies on the scattered signal; however, at the same time, energy is effectively lost by the scattering.

Variations in the relative importance of scattering strength and scattering loss are evident in the relationship between working range and wind speed (Fig. 6). Working range increases over the range of $0.5\,\mathrm{m\,s^{-1}} < |U_{10}| < 6.5\,\mathrm{m\,s^{-1}}$, implying that the increase in scattering strength must dominate over the increased loss. At higher wind speeds, the range does not change—and even slightly decreases. This plateau might reflect the transition to a state whereby the scattering loss becomes increasingly important relative to the scattering target strength. In fact, the Sverdrup–Munk–Bretschneider (SMB) growth curves predict that the significant wave height, which represents scattering loss, increases nearly linearly over the range of observed wind speeds, whereas the JONSWAP spectrum predicts that the Bragg wave spectral energy at 6 m, which represents target strength, saturates at only about $U_{10} = 4\,\mathrm{m\,s^{-1}}$. In other words, the scattering loss increases more rapidly at higher wind speeds than the scattering strength in fetch-limited seas.

The working range is lower under northwesterly winds than under southeasterly winds when the speed is greater than about $5\,\mathrm{m\,s^{-1}}$ (Fig. 6). The reduced range is at least partly due to differences in fetch associated with each wind direction. The fetch under northwesterly winds is about 60 km, while the fetch under southeasterly winds is about 50 km, although it could be as low as 10 km for an easterly wind. Using the SMB growth curves and the JONSWAP spectrum, we find that the fetch difference means that the significant wave height under northwesterly winds compared to southeasterly winds can be 8%–119% larger, while the Bragg spectral energy is 3%–15% *lower* at $U_{10} = 10\,\mathrm{m\,s^{-1}}$. In other words, the loss term increases with fetch, while the target strength decreases.

The wind direction is expected to affect the directionality of the wave field, which in turn will affect the first-order line strength (Barrick 1972). Heron and Rose (1986) and Shen et al. (2012) inverted this principle to determine wind direction from first-order line strength. Waves traveling parallel to the radar bearing will create stronger echoes than waves traveling in other directions. Assessing the importance of wave direction on working range relies on a somewhat detailed knowledge of the

wave field. A simple assumption would be that the wave field follows the wind; however, applying this assumption requires that the Sand Heads wind record is representative of the wind field over the region of wave generation and that the wave components of interest precisely follow the wind direction. Unfortunately, we cannot test these either of these assumptions because there are no wave measurements available in the CODAR footprint and there are limited wind stations.

The relative importance of scattering loss and scattering strength, and wave direction, are not the only aspects of sea state that can affect the working range. For example, Cosoli et al. (2010) observe elevated levels of Doppler spectrum broadband noise in response to high wind speeds and large significant waves, and they attribute a reduction in working range to the increased noise. Gurgel et al. (1999a) point out that nonlinear effects (e.g., wave breaking), not accounted for in linear scattering theory, become increasingly important at high wind speeds.

d. Tides

The Welch periodogram shown in Fig. 7 confirmed that the working range contains tidal fluctuations and that the conditional averages of range at various elevations reveal a weak correlation between range and sea surface elevation (Fig. 8). The estimated impact is that the working range increases by 3 km over the 5-m increase of sea surface elevation, meaning that the tidal impact is weaker than the wave and conductivity effects.

Even though the effect of a variable sea level appears to be weak, there are a number of reasons to expect a causal relationship. First, the outflow from the Fraser River is tidally pulsed, and the lowest salinity is generally found at low water, particularly during early summer, when the river flow is high and low tides are more pronounced (Halverson and Pawlowicz 2008). At low tides, a plume of brackish water expands into the HF radar footprint, causing a reduction in the near-surface salinity and therefore conductivity. These conductivity fluctuations are about $\pm 0.1\,\mathrm{S\,m^{-1}}$ (Fig. 3b), which, using the slope of the conductivity–range regression (Fig. 4), would yield a working range variability of about $\Delta R = \pm 0.1\,\mathrm{S\,m^{-1}} \times (7\,\mathrm{km}/1\,\mathrm{S\,m^{-1}}) = \pm 0.7\,\mathrm{km}$.

Tides determine the amount of land between the antenna and the shore, and also set the height of the antenna relative to sea level. Land attenuates EM waves to a much greater degree than seawater because it has a lower conductivity and permittivity (e.g., Fernandez et al. 2000). Thus, at low tide, more energy is lost to land than at high tide, reducing the working range. Unfortunately, the Westshore HF radar station is not publicly accessible, so we were unable to visit the site to assess the tidal effects on the foreshore. We note, however, that the instrument is located at a major shipping port, equipped to handle deep draft container ships, so the tidal changes to the foreshore are likely minimal.

The last tidal elevation factor that might be important is that the amount of radiated (and received) EM energy decreases as the height of the antenna above the surface increases (e.g., Norton 1936). This means that, for example, less energy would be ultimately radiated (and received) at low tide.

In section 3d the possibility that tidal currents might have an impact on working range was discussed. Support for this comes from the $r \approx 1.5$ h lead of working range relative to sea surface height. This means that the range varies in phase with the tidal currents because the tidal currents peak between high and low water. It is not clear, however, how the current speed can affect the working range. In terms of the radar spectrum, the current speed determines the Doppler bin in which the target occurs, and not the strength of the echo.

While it is unlikely that the current speed directly impacts the working range, a tidal signal could be introduced if the surface Bragg wave amplitude was modulated by the tides. There are at least two ways this could occur. First, there could be a tidal modulation of the relative speed between the wind and the water. Suppose southeasterly winds blow consistently over one semidiurnal tidal cycle. Ebb tides flow to the southeast in the SoG, meaning southeasterly winds oppose ebb currents, which would have the effect of increasing the surface wave amplitude because the relative speed between the wind and water is higher. During flood tide, the wind and tidal flow are in the same direction, reducing the relative speed between the wind and water, and thus the wave height. We can use the slope of the working range and wind speed regression in Fig. 6 to estimate the magnitude of the effect. A tidal current of $0.5\,\mathrm{m\,s^{-1}}$ oscillating around a relatively weak wind would change the working range by about $\Delta R = \pm 0.5\,\mathrm{m\,s^{-1}} \times (1\,\mathrm{km}/1\,\mathrm{m\,s^{-1}}) = \pm 0.5\,\mathrm{km}$. Thus, the range could change by as much as 1 km over a tidal cycle by this effect.

A second mechanism that generates tidal modulations of the wave field occurs as a result of wave–current interactions. A well-known result of wave–current theory is that the wave spectrum is modified by spatially or temporally variable currents. When the currents flow in the opposite direction to the waves, wave spectral energy levels increase, and when the currents flow in the same direction as the waves, wave spectral energy levels decrease. Support for both tidal modulation effects discussed here is found in a periodogram of the Halibut Bank buoy spectral energy at $f = 0.4512$ Hz, which contains both semidiurnal and diurnal tidal lines (not shown).

While the semidiurnal variations are tidal in nature (perhaps by interacting with sea state and wind), we stated in section 4d that the strong diurnal energy centered at the frequency of S_1 (Fig. 7) is not caused by the tides because S_1 is weak in the sea level record. However, a periodogram of Sand Heads wind speed contains energy at S_1 (not shown). Thus, it seems more likely that the diurnal fluctuation in range is caused by the modulation of Bragg wave energy by the sea breeze.

e. Limitations to the analysis

1) HIGH-FREQUENCY RADIO NOISE

Thus far we have focused on some environmental factors that determine the strength of the signal. However, noise levels can vary and affect the working range (Shearman 1983). Noise originates from within the instrumentation itself and from external sources. Internal noise is caused by electrical and thermal noise sources (Meadows et al. 2013). External noise is caused by natural events, such as lightning, auroral activity, or astronomical phenomena (e.g., by pulsars, radio galaxies, Jupiter, the sun), and it is caused by man-made sources [e.g., amplitude modulation (AM) radio, citizens band (CB) radios]. Internal noise is generally considered to be insignificant compared to external noise.

Identifying whether noise fluctuations make an important contribution to the SNR is not trivial when the noise level itself is not explicitly analyzed. However, time variations in the working range or data coverage area can provide some insight if there is no reason to expect the signal itself to vary. For example, diurnal variance in the working range and data coverage were found to be caused by the diurnal fluctuation of ionospheric D-layer absorption of HF radio waves (Shearman 1983; Chavanne et al. 2010; Savidge et al. 2011; Meadows et al. 2013). Diurnal variations are important to working range in this study (Fig. 7); however, ionospheric variability is generally most problematic at lower high frequencies (≈5 MHz; Shearman 1983).

At higher frequencies in the HF band, galactic and solar radio sources or man-made communications might generate appreciable noise. However, these sources are not necessarily periodic, nor do we have any information on these sources against which to compare the working range time series. Investigation into the importance of noise from these sources remains to be carried out, and it likely requires some knowledge of the sources and an explicit analysis of the measured noise rather than the SNR or range.

2) PATH LOSS, SNR, AND WORKING RANGE

In this study we chose to characterize the working range by finding the distance to the farthest radial solution, rather than considering, for example, SNR or path loss. The drawback of this approach is that the instrument configuration and data processing steps become relevant, meaning that the working range could depend not only on environmental factors, but also on instrument configuration (e.g., Bragg threshold SNR). The threshold SNR factor for the first-order Bragg peak was set to 4 (6 dB), which is the default setting recommended by the vendor. For transparency, the appendix contains a radial file header to show how the instrument was configured for this study.

6. Conclusions

The working range for radial current measurements was found to vary with conductivity, sea state, and tides, which account for 34%, 16%, and 14% (or less) of the total variance, respectively. Working range increases nearly linearly with conductivity. The dependence on wind speed is linear at low wind speeds; however, it peaks and subsequently decreases at the highest speeds. The relationship of the working range to the tides is not as clear; however, the range leads sea level by about 1.5 h which, as was discussed, implies that tidal currents are likely responsible. The remaining unexplained variance is probably due to the use of wind speed as a proxy for sea state, which contains errors, and a correlation between some predictors (e.g., low conductivity at low tide). Errors are also expected from the MUSIC algorithm used by the vendor for direction finding.

While conductivity variations had the largest impact, they should not be considered a limiting factor in the range. Working ranges of 30 km can still be achieved under low-salinity conditions (say, $S_R = 15\,\mathrm{g\,kg^{-1}}$). It is essentially impossible for conductivity to approach freshwater values in the ocean, which means a highly conductive medium will always be present. The salinity in the Fraser River plume under freshet is lower than is found in most coastal regions, except for perhaps the Baltic Sea, or the near-field region of some river plumes, such as the Columbia or Merrimack Rivers. This means that salinity will not limit the working range of most HF radar installations.

Instead, the limiting factor for most systems, at least at 25 MHz in fetch-limited waters, is sea state. In the Strait of Georgia, at the Sand Heads light station, only 25% of the wind speeds exceed $6.5\,\mathrm{m\,s^{-1}}$—the minimum speed required to maximize working range. This means that the range is limited by sea state 75% of the time in the Strait of Georgia.

Tidal variations in working range affect the working range by a number of mechanisms: first, tides modulate sea state; second, tides modulate the river discharge and therefore the salinity of the river plume. Finally, local tidal variations in the foreshore environment, and the

variable height of the system above sea level, might also play a role.

Acknowledgments. Funding was provided by MEOPAR, one of the Canadian Natural Sciences and Engineering Research Council's (NSERC) Networks of Centres of Excellence (NCE). This study was mostly based on data collected by Ocean Networks Canada and was distributed by the freely accessible Ocean Networks Canada Data Archive (http://www.oceannetworks.ca), Oceans Networks Canada, University of Victoria, Canada. The data were downloaded at various times from June 2014 onward, and we worked closely with Ocean Networks Canada staff scientists and data specialists to ensure we were provided with the most up-to-date and highest-quality data available. In particular we wish to thank Kevin Bartlett and Marlene Jeffries. Maeve Daugharty and Don Barrick of CODAR Ocean Sensors provided the numerical prediction of working range versus conductivity.

APPENDIX

System Configuration Parameters

Header from an hourly radial file at the Westshore site (VCOL) to exemplify instrument settings in this study.

```
%CTF: 1.00
%FileType: LLUV rdls "RadialMap"
%LLUVSpec: 1.18 2012 05 07
%UUID: 7D75019D-C92C-4F38-B109-F7EF5979F303
%Manufacturer: CODAR Ocean Sensors. SeaSonde
%Site: VCOL ""
%TimeStamp: 2014 06 05 00 00 00
%TimeZone: "UTC" +0.000 0 "UTC"
%TimeCoverage: 75.000 Minutes
%Origin: 49.0180500-123.1718833
%GreatCircle: "WGS84" 6378137.000 298.257223562997
%GeodVersion: "CGEO" 1.57 2009 03 10
%LLUVTrustData: all %% all lluv xyuv rbvd
%RangeStart: 3
%RangeEnd: 54
%RangeResolutionKMeters: 0.500300
%AntennaBearing: 278.0 True
%ReferenceBearing: 0 True
%AngularResolution: 5 Deg
%SpatialResolution: 5 Deg
%PatternType: Measured
%PatternDate: 2012 01 18 17 44 43
%PatternResolution: 1.0 deg
%PatternSmoothing: 20.0 deg
%PatternUUID: E51B66E9-209C-454D-8A62-D774B57F576A
%TransmitCenterFreqMHz: 24.400000
%DopplerResolutionHzPerBin: 0.001953125
%FirstOrderMethod: 0
%BraggSmoothingPoints: 5
%CurrentVelocityLimit: 85.0
%BraggHasSecondOrder: 1
%RadialBraggPeakDropOff: 501.190
%RadialBraggPeakNull: 79.430
%RadialBraggNoiseThreshold: 4.000
%PatternAmplitudeCorrections: 3.2853 0.7716
%PatternPhaseCorrections: -139.40-136.40
%PatternAmplitudeCalculations: 1.3193 0.7610
%PatternPhaseCalculations: -158.50-141.10
%RadialMusicParameters: 40.000 20.000 2.000
%MergedCount: 6
%RadialMinimumMergePoints: 2
%FirstOrderCalc: 1
%MergeMethod: 1 MedianVectors
%MergeMethod: 1 MedianVectors
%PatternMethod: 1 PatternVectors
%TransmitSweepRateHz: 4.000000
%TransmitBandwidthKHz: -299.616272
%SpectraRangeCells: 79
%SpectraDopplerCells: 2048
%TableType: LLUV RDL9
%TableColumns: 18
%TableColumnTypes: LOND LATD VELU VELV VFLG ESPC ETMP MAXV MINV ...
ERSC ERTC XDST YDST RNGE BEAR VELO HEAD SPRC
%TableRows: 1398
%TableStart:
```

REFERENCES

Barrick, D. E., 1971a: Theory of HF and VHF propagation across the rough sea, 1: The effective surface impedance for a slightly rough highly conducting medium at grazing incidence. *Radio Sci.*, **6**, 517–526, doi:10.1029/RS006i005p00517.

——, 1971b: Theory of HF and VHF propagation across the rough sea, 2: Application to HF and VHF propagation above the sea. *Radio Sci.*, **6**, 527–533, doi:10.1029/RS006i005p00527.

——, 1972: First-order theory and analysis of MF/HF/VHF scatter from the sea. *IEEE Trans. Antennas Propag.*, **20**, 2–10, doi:10.1109/TAP.1972.1140123.

——, 1977: Extraction of wave parameters from measured HF radar sea-echo Doppler spectra. *Radio Sci.*, **12**, 415–424, doi:10.1029/RS012i003p00415.

——, M. W. Evans, and B. L. Weber, 1977: Ocean surface currents mapped by radar. *Science*, **198**, 4313, 138–144, doi:10.1126/science.198.4313.138.

Chavanne, C., P. Flament, G. Carter, M. Merrifield, D. Luther, E. Zaron, and K.-W. Gurgel, 2010: The surface expression of semidiurnal internal tides near a strong source at Hawaii. Part I: Observations and numerical predictions. *J. Phys. Oceanogr.*, **40**, 1155–1179, doi:10.1175/2010JPO4222.1.

Cosoli, S., A. Mazzoldi, and M. Gačić, 2010: Validation of surface current measurements in the northern Adriatic Sea from high-frequency radars. *J. Atmos. Oceanic Technol.*, **27**, 908–919, doi:10.1175/2009JTECHO680.1.

Crombie, D. D., 1955: Doppler spectrum of sea echo at 13.56 Mc./s. *Nature*, **175**, 681–682, doi:10.1038/175681a0.

Fernandez, D., L. Meadows, J. Vesecky, C. Teague, J. Paduan, and P. Hansen, 2000: Surface current measurements by HF radar in freshwater lakes. *IEEE J. Oceanic Eng.*, **25**, 458–471, doi:10.1109/48.895353.

Foreman, M., R. Walters, R. Henry, C. Keller, and A. Dolling, 1995: A tidal model for Juan-de-Fuca Strait and the Southern Strait of Georgia. *J. Geophys. Res.*, **100**, 721–740, doi:10.1029/94JC02721.

Forget, P., and P. Broche, 1991: A study of VHF radio wave propagation over a water surface of variable conductivity. *Radio Sci.*, **26**, 1229–1237, doi:10.1029/91RS01413.

——, ——, and J. C. de Maistre, 1982: Attenuation with distance and wind speed of HF surface waves over the ocean. *Radio Sci.*, **17**, 599–610, doi:10.1029/RS017i003p00599.

Gurgel, K.-W., H.-H. Essen, and S. Kingsley, 1999a: High-frequency radars: Physical limitations and recent developments. *Coastal Eng.*, **37**, 201–218, doi:10.1016/S0378-3839(99)00026-5.

——, ——, and T. Schlick, 1999b: Tracking of fresh-water plumes in Dutch coastal waters by means of HF radar. *IGARSS'99 Proceedings: Remote Sensing of the System Earth—A Challenge for the 21st Century*, T. I. Stein, Ed., Vol. 5, IEEE, 2548–2550, doi:10.1109/IGARSS.1999.771572.

Halverson, M. J., 2009: Multi-timescale analysis of the salinity and algal biomass of the Fraser River plume from repeated ferry transects. Ph.D. thesis, University of British Columbia, 181 pp., doi:10.14288/1.0053481.

——, and R. Pawlowicz, 2008: Estuarine forcing of a river plume by river flow and tides. *J. Geophys. Res.*, **113**, C090330, doi:10.1029/2008JC004844.

——, and ——, 2011: Entrainment and flushing time in the Fraser River estuary and plume from a steady salt balance analysis. *J. Geophys. Res.*, **116**, C08023, doi:10.1029/2010JC006793.

——, and S. W. Fleming, 2015: Complex network theory, streamflow, and hydrometric monitoring system design. *Hydrol. Earth Syst. Sci.*, **19**, 3301–3318, doi:10.5194/hess-19-3301-2015.

——, and R. Pawlowicz, 2016: Tide, wind, and river forcing of the surface currents in the Fraser River plume. *Atmos.–Ocean*, **54**, 131–152, doi:10.1080/07055900.2016.1138927.

Hansen, P., 1977: Measurements of basic transmission loss for HF ground wave propagation over seawater. *Radio Sci.*, **12**, 397–404, doi:10.1029/RS012i003p00397.

Hasselmann, K., 1971: Determination of ocean wave spectra from Doppler radio return from the sea surface. *Nature*, **229**, 16–17, doi:10.1038/physci229016a0.

Heron, M., and R. Rose, 1986: On the application of HF ocean radar to the observation of temporal and spatial changes in wind direction. *IEEE J. Oceanic Eng.*, **11**, 210–218, doi:10.1109/JOE.1986.1145173.

Hinatsu, M., Y. Tsukada, H. Tomita, and A. Harashima, 2004: Study on estimation of original location of water sampled through inlet set on volunteer observing ship. *J. Adv. Mar. Sci. Technol. Soc.*, **9**, 37–46.

IOC, SCOR, and IAPSO, 2010: The International Thermodynamic Equation of Seawater—2010: Calculations and use of thermodynamic properties. Intergovernmental Oceanographic Commission Manuals and Guides 56, 207 pp.

Kamli, E., C. Chavanne, and D. Dumont, 2016: Experimental assessment of the performance of high-frequency CODAR and WERA radars to measure ocean currents in partially ice-covered waters. *J. Atmos. Oceanic Technol.*, **33**, 539–550, doi:10.1175/JTECH-D-15-0143.1.

Lyons, R. S., and D. E. Barrick, 1984: Attenuation rates of coastal radar signals at 25 MHz. *Radio Sci.*, **19**, 319–324, doi:10.1029/RS019i001p00319.

Meadows, L. A., C. Whelan, D. Barrick, R. Kroodsma, C. Ruf, C. C. Teague, G. A. Meadows, and S. Wang, 2013: High frequency radar and its application to fresh water. *J. Great Lakes Res.*, **39** (Suppl. 1), 183–193, doi:10.1016/j.jglr.2013.01.002.

Meulé, S., P. Hill, and C. Pinazo, 2007: Wave dynamics over Roberts Bank, British Columbia: Processes and modelling. Geological Survey of Canada Tech. Rep. 2007-A11, 9 pp., doi:10.4095/224297.

Norton, K. A., 1936: The propagation of radio waves over the surface of the Earth and in the upper atmosphere. *Proc. Inst. Radio Engr.*, **24**, 1367–1387, doi:10.1109/JRPROC.1936.227360.

Pawlowicz, R., 2015: The absolute salinity of seawater diluted by riverwater. *Deep-Sea Res. I*, **101**, 71–79, doi:10.1016/j.dsr.2015.03.006.

——, O. Riche, and M. Halverson, 2007: The circulation and residence time of the Strait of Georgia using a simple mixing-box approach. *Atmos.–Ocean*, **45**, 173–193, doi:10.3137/ao.450401.

Royer, L., and W. Emery, 1982: Variations of the Fraser River plume and their relationship to forcing by tide, wind and discharge. *Atmos.–Ocean*, **20**, 357–372, 9649151, doi:10.1080/07055900.1982.9649151.

Savidge, D., J. Amft, A. Gargett, M. Archer, D. Conley, G. Voulgaris, L. Wyatt, and K.-W. Gurgel, 2011: Assessment of WERA long-range HF-radar performance from the user's perspective. *2011 IEEE/OES/CWTM Tenth Working Conference on Current, Waves and Turbulence Measurements* (CWTM), J. Rizoli White and A. J. Williams III, Eds., IEEE, 31–38, doi:10.1109/CWTM.2011.5759520.

Shearman, E., 1983: Propagation and scattering in MF/HF groundwave radar. *IEE Proc.*, **130F**, 579–590, doi:10.1049/ip-f-1:19830092.

Shen, W., K.-W. Gurgel, G. Voulgaris, T. Schlick, and D. Stammer, 2012: Wind-speed inversion from HF radar first-order backscatter signal. *Ocean Dyn.*, **62**, 105–121, doi:10.1007/s10236-011-0465-9.

Smith, S. D., 1988: Coefficients for sea surface wind stress, heat flux, and wind profiles as a function of wind speed and temperature. *J. Geophys. Res.*, **93**, 15 467–15 472, doi:10.1029/JC093iC12p15467.

Stewart, R. H., and J. W. Joy, 1974: HF radio measurement of surface currents. *Deep-Sea Res. Oceanogr. Abstr.*, **21**, 1039–1049, doi:10.1016/0011-7471(74)90066-7.

Thomson, R. E., 1981: *Oceanography of the British Columbia Coast*. Canadian Special Publications of Fisheries and Aquatic Sciences, Vol. 56, Dept. of Fisheries and Oceans, Institute of Ocean Sciences, 291 pp.

Wang, C., 2015: Oxygen budgets and productivity estimates in the Strait of Georgia from a continuous ferry-based monitoring system. M.S. thesis, Dept. of Earth, Ocean, and Atmospheric Sciences, University of British Columbia, 124 pp.